

# Interaction and collision of skyrmions in chiral antiferromagnets

George Theodorou<sup>1,2</sup> and Stavros Komineas<sup>1,2</sup>

<sup>1</sup> *Department of Mathematics and Applied Mathematics, University of Crete, 70013 Heraklion, Greece*

<sup>2</sup> *Institute of Applied and Computational Mathematics, Foundation for Research and Technology - Hellas (FORHT), Nikolaou Plastira 100, Vassilika Vouton, 70013 Heraklion, Greece*

---

## Abstract

Skyrmions in an antiferromagnet can travel as solitary waves in stark contrast to the situation in ferromagnets. Traveling skyrmion solutions have been found numerically in chiral antiferromagnets. We consider head-on collision events between two skyrmions. We find that the result of the collision depends on the initial velocity of the skyrmions. For small velocities, the skyrmions are shrinking as they are approaching, they bounce back and eventually acquire almost their initial speed. For larger velocities, the skyrmions approach each other and shrink until they become singular points and are eventually annihilated. We describe the observed phenomena in terms of skyrmion energetics and thus determine the regimes of the different dynamical behaviors.

---

## 1. Introduction

Antiferromagnets (AFM) present magnetic ordering but no net magnetization, in contrast to ferromagnets (FM). As a result, no stray fields are produced and they are robust against moderate external magnetic fields. Their dynamics, such as spin wave frequencies and switching timescales, are in the THz range. These qualities, combined with the fact that antiferromagnetic materials are abundant, make them very interesting to study. While in the previous decades, antiferromagnetic order had proven difficult to detect and manipulate, interest in antiferromagnetic materials is burgeoning since experimental techniques now allow for optical switching of magnon modes [1, 2, 3, 4], optical [5, 6, 7] or phonon-based manipulation [8], and electrical [9, 10, 11] or current-induced switching of antiferromagnetic domains [11, 12], spin dynamics in the THz range [13, 14, 15], observation of AFM domain walls and their dynamics [16].

The microscopic description of AFM order is formally analogous to the standard description of ferromagnets [17]. Skyrmions and other topological magnetic excitations are expected to form in antiferromagnets in complete analogy to ferromagnets [18, 19, 20]. Specific skyrmionic (meronic) textures have been observed [21, 22]. AFM skyrmions stand out due to their solitary wave dynamics [23, 24]. The solitary wave character of skyrmions in AFM gives them particle-like properties and they behave as Newtonian or relativistic particles for low and large velocities, respectively. This allows them to be driven to large speeds, e.g., by spin torques [25, 26]. In chiral antiferromagnets, they are seen to get elongated as they are accelerated [25, 27], a phenomenon that has been linked to the spiral phase transition [24]. A detailed description of the shape and profile of propagating skyrmions and a full explanation of the phenomenon remain elusive.

In the present paper, we study skyrmion interactions, specifically, the result of a collision between two skyrmions. Collisions of solitons in field theories, mainly applied to particle physics, have revealed surprising behaviors. Two solitons in two or three space dimensions that are colliding are often seen to scatter at right angles [28, 29, 30]. This is observed, for example, within the  $O(3)$  nonlinear sigma model [31], which is used in particle physics but it is also a simplified model for the antiferromagnetic structure.

In the present model, we find that two propagating skyrmions that collide head-on will initially shrink while they are decelerated. At the same time, their configuration changes from elongated to nearly circular. There are two possible outcomes. Slowly moving skyrmions, will eventually stop temporarily and bounce back. Skyrmions with larger velocities will shrink completely while approaching each other and they will be annihilated. We discuss the emerging kinetic energy of the spin system that plays a central role in the phenomenon.

The paper is organized as follows. Section 2 gives a review of the main results for the solitary wave motion of skyrmions. Section 3 contains numerical simulations and a theoretical description of skyrmion collision events. Section 4 contains our concluding remarks. In Appendix A, we derive formulas for the energy terms, specifically, formulas in the discrete lattice for the kinetic energy of the skyrmion that is important for the collision dynamics.

## 2. Traveling skyrmions

We study a two-dimensional system and a square lattice of spins  $\mathbf{S}_{i,j}$  with a fixed length  $S_{i,j}^2 = s^2$ , where  $i, j$  are integer indices for the spin site. A discrete Hamiltonian on the lattice includes symmetric exchange, a Dzyaloshinskii-Moriya (DM), and an easy-axis anisotropy term,  $E^d = E_{\text{ex}}^d + E_{\text{DM}}^d + E_{\text{a}}^d$ , with

$$\begin{aligned} E_{\text{ex}}^d &= J \sum_{i,j} \mathbf{S}_{i,j} \cdot (\mathbf{S}_{i+1,j} + \mathbf{S}_{i,j+1}), \\ E_{\text{DM}}^d &= D \sum_{i,j} [\hat{\mathbf{e}}_2 \cdot (\mathbf{S}_{i,j} \times \mathbf{S}_{i+1,j}) - \hat{\mathbf{e}}_1 \cdot (\mathbf{S}_{i,j} \times \mathbf{S}_{i,j+1})], \\ E_{\text{a}}^d &= -\frac{K}{2} \sum_{i,j} [(\mathbf{S}_{i,j})_z]^2, \end{aligned} \quad (1)$$

where  $\hat{\mathbf{e}}_\mu$ ,  $\mu = 1, 2, 3$  denote the unit vectors in spin space,  $(\mathbf{S}_{i,j})_z$  is the out-of-plane component of a spin vector, and  $J, D, K$  are positive constants. The equations of motion for each spin are derived from the energy and have the form

$$\frac{\partial \mathbf{S}_{i,j}}{\partial t} = -\mathbf{S}_{i,j} \times \frac{\partial E}{\partial \mathbf{S}_{i,j}} \quad (2)$$

where the effective field is

$$\begin{aligned} -\frac{\partial E^d}{\partial \mathbf{S}_{i,j}} &= -J(\mathbf{S}_{i+1,j} + \mathbf{S}_{i,j+1} + \mathbf{S}_{i-1,j} + \mathbf{S}_{i,j-1}) \\ &+ D [\hat{\mathbf{e}}_2 \times (\mathbf{S}_{i+1,j} - \mathbf{S}_{i-1,j}) - \hat{\mathbf{e}}_1 \times (\mathbf{S}_{i,j+1} - \mathbf{S}_{i,j-1})] + K(\mathbf{S}_{i,j})_z \hat{\mathbf{e}}_3. \end{aligned} \quad (3)$$

A continuum model for the antiferromagnet will facilitate the analysis and it will offer significant insight into the dynamics. We consider a tetramerization of the square lattice and define the four linear combinations of the spins at each tetramer [19, 24],

$$\begin{aligned} \mathbf{m} &= \frac{1}{4s} (\mathbf{S}_{i,j} + \mathbf{S}_{i+1,j} + \mathbf{S}_{i+1,j+1} + \mathbf{S}_{i,j+1}), & \mathbf{n} &= \frac{1}{4s} (\mathbf{S}_{i,j} - \mathbf{S}_{i+1,j} + \mathbf{S}_{i+1,j+1} - \mathbf{S}_{i,j+1}), \\ \mathbf{k} &= \frac{1}{4s} (\mathbf{S}_{i,j} + \mathbf{S}_{i+1,j} - \mathbf{S}_{i+1,j+1} - \mathbf{S}_{i,j+1}), & \mathbf{l} &= \frac{1}{4s} (\mathbf{S}_{i,j} - \mathbf{S}_{i+1,j} - \mathbf{S}_{i+1,j+1} + \mathbf{S}_{i,j+1}). \end{aligned} \quad (4)$$

A small parameter  $\epsilon$  is introduced that will control the continuum approximation. The scaled space and time variables are defined as

$$x = \epsilon i, \quad y = \epsilon j, \quad \tau = 2\sqrt{2}\epsilon s J t. \quad (5)$$

The continuum model is written entirely in terms of the Néel vector  $\mathbf{n} = \mathbf{n}(x, y, \tau)$  with components  $(n_1, n_2, n_3)$ , which satisfies the local constraint  $|\mathbf{n}| = 1$ . This obeys an extension of the  $\sigma$  model [17, 19],

$$\mathbf{n} \times (\dot{\mathbf{n}} - \mathbf{f}) = 0, \quad \mathbf{f} = \Delta \mathbf{n} + 2\lambda \epsilon_{\mu\nu} \hat{\mathbf{e}}_\mu \times \partial_\nu \mathbf{n} + n_3 \hat{\mathbf{e}}_3, \quad \lambda = \frac{D}{\sqrt{KJ}} \quad (6)$$

where the dot denotes differentiation with respect to the scaled time  $\tau$ ,  $\Delta$  denotes the Laplacian in two dimensions,  $\epsilon_{\mu\nu}$  is the antisymmetric tensor with  $\mu, \nu = 1, 2$ , and the summation convention for repeated indices is adopted. The notation  $\partial_1, \partial_2$  denotes differentiation with respect to  $x, y$  respectively. In deriving model (6), the choice has been made

$$\epsilon = \sqrt{\frac{K}{J}}. \quad (7)$$

The fields  $\mathbf{m}, \mathbf{k}, \mathbf{l}$  are auxiliary and they are given in terms of  $\mathbf{n}$  as

$$\mathbf{m} = \frac{\epsilon}{2\sqrt{2}} \mathbf{n} \times \dot{\mathbf{n}}, \quad \mathbf{k} = -\frac{\epsilon}{2} \partial_1 \mathbf{n}, \quad \mathbf{l} = -\frac{\epsilon}{2} \partial_2 \mathbf{n}. \quad (8)$$

The system is Hamiltonian with energy  $E = E_{\text{kin}} + V$ , where the kinetic and potential energies are

$$E_{\text{kin}} = \frac{1}{2} \int \dot{\mathbf{n}}^2 d^2x, \quad V = E_{\text{ex}} + E_{\text{DM}} + E_{\text{a}} \quad (9)$$

$$E_{\text{ex}} = \frac{1}{2} \int (\partial_\mu \mathbf{n}) \cdot (\partial_\mu \mathbf{n}) d^2x, \quad E_{\text{DM}} = -\lambda \int \epsilon_{\mu\nu} \hat{\mathbf{e}}_\mu \cdot (\partial_\nu \mathbf{n} \times \mathbf{n}) d^2x, \quad E_{\text{a}} = \frac{1}{2} \int (1 - n_3^2) d^2x.$$

The effective field in Eq. (6) is derived from  $\mathbf{f} = -\delta V / \delta \mathbf{n}$ .

The static sector of the  $\sigma$  model (6) for the Néel vector is identical to the static sector of the Landau-Lifshitz equation for the magnetization vector of a ferromagnet with corresponding interactions. Therefore, static skyrmions are obtained in an AFM for parameter values  $\lambda < 2/\pi$ . For  $\lambda > 2/\pi$ , a spiral is the ground state.

Skyrmions traveling with velocity  $v$  are solutions of Eq. (6) of the form

$$\mathbf{n}_v(\xi, \eta) = \mathbf{n}(x - v\tau, y), \quad \xi = x - v\tau, \quad \eta = y \quad (10)$$

where we have chosen  $x$  as the direction of propagation. The skyrmion velocity can take values in the range  $0 \leq v < v_c \equiv \sqrt{1 - (\pi\lambda/2)^2}$  [24].

We have simulated numerically the solitary wave motion of a skyrmion. We consider a solution (10) of the continuum model (6) as obtained in [24]. The auxiliary fields are given by (8), e.g., we have  $\mathbf{m} = -\frac{\epsilon v}{2\sqrt{2}} \mathbf{n} \times \partial_1 \mathbf{n}$  with  $\mathbf{n} = \mathbf{n}_v$ . We use finite differences and apply the configuration on a lattice for the variables (4). The corresponding spin variables are obtained by inverting Eq. (4) on a numerical mesh. The simulations are performed using Eqs. (2) for the spins. We typically use the parameter values

$$J = 1, \quad D = 0.015, \quad K = 0.0009. \quad (11)$$

Then, Eq. (7) gives  $\epsilon = 0.03$  and Eq. (6) gives  $\lambda = 0.50$ . If we have a velocity  $v$  in the scaled variables used in the continuum, then we expect a skyrmion velocity  $v^d$  in the simulation lattice, given via

$$v = \frac{\Delta x}{\Delta \tau} = \frac{\epsilon \Delta i}{2\sqrt{2}\epsilon \Delta t} = \frac{v^d}{2\sqrt{2}}, \quad v^d = \frac{\Delta i}{\Delta t}. \quad (12)$$

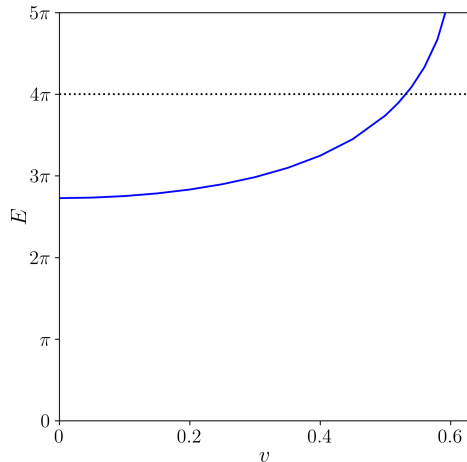


Figure 1: Energy  $E$  of propagating skyrmions of the form (10) as a function of velocity  $v$  for parameter value  $\lambda = 0.50$ . The static skyrmion ( $v = 0$ ) has energy  $E < 4\pi$ . The energy crosses the critical value  $E = 4\pi$  at  $v \approx 0.53$ .

Numerical simulations verify that a traveling skyrmion, as calculated in the continuum model, is propagating coherently with the expected velocity in the spin lattice. We measure an error in the expected velocity approximately 2% for initial velocity  $v = 0.2$  and 1% for initial velocity  $v = 0.4$ .

The energy terms play an important role in the interpretation of the simulation results. For this purpose, we need to obtain the relation between the discrete, Eq. (1), and the continuum, Eq. (9), energy terms. We also need formulas to approximate the continuum energy terms on the numerical mesh. These are derived in Appendix A. The main new element is formula (A.4) for the kinetic energy calculated in terms of spin variables. Fig. 1 gives the energy of propagating skyrmions versus their velocity for  $\lambda = 0.50$ , calculated numerically. The value  $4\pi$  is the minimum exchange energy possible. A static skyrmion has total energy  $E < 4\pi$  due to the negative contribution of the DM term. In the limit of a small radius (obtained for small  $\lambda$ ), the energy of a static skyrmion approaches the value  $E = 4\pi$  [32, 33]. The energy of a traveling skyrmion becomes  $E > 4\pi$  for a large enough velocity, for example, for  $v > 0.53$  when  $\lambda = 0.50$ . This is a critical velocity value because skyrmions with energy greater than  $4\pi$  can potentially shrink to become singular configurations and thus physically disappear [34].

### 3. Collisions of skyrmions

Propagating skyrmions in antiferromagnets can be obtained through acceleration induced by an energy gradient. This can be produced by, e.g., an anisotropy gradient [35] or any other variation of the material properties. One could consider a voltage that would change the anisotropy or DM strength locally. If two (or more) skyrmions are at rest, a local change in the magnetic energy would cause an acceleration of both skyrmions towards the lowest energy region. If this region is between them, that would automatically set the skyrmions on a head-on collision course. This situation can be compared with collisions of skyrmions in ferromagnets that have to be manipulated [36] and cannot occur spontaneously.

We will set up our system assuming that the two skyrmions are moving toward each other with an initial velocity and they are in a homogeneous background (that is, any voltage that was initially applied in order

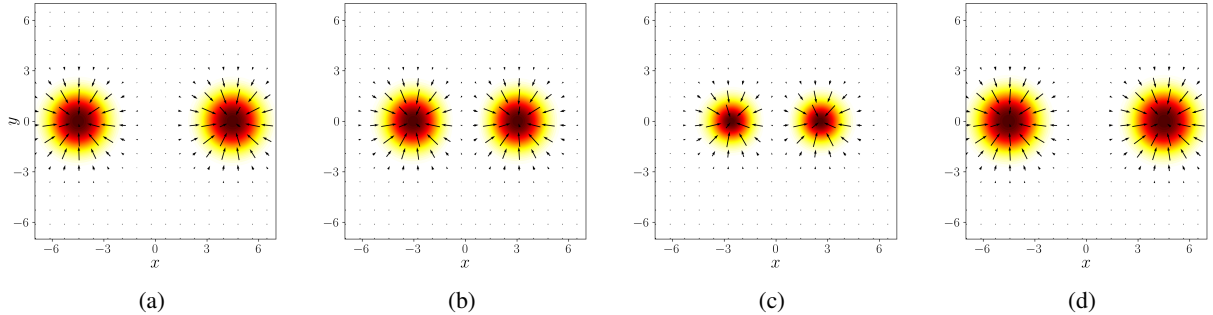


Figure 2: Simulation of a head-on collision of skyrmions placed initially ( $\tau = 0$ ) at positions  $(\pm 10.5, 0)$  with velocities  $v = \mp 0.2$ . (a) At the time  $\tau = 30.0$ , the skyrmions are at a distance, not yet interacting. (b) At  $\tau = 38.0$ , their velocities and sizes have decreased due to interaction. (c) At  $\tau = \tau_{\text{crit}} = 46.2$ , they stop ( $v = 0$ ) temporarily and have a minimum size. (d) At  $\tau = 60.8$ , they have bounced back and they have acquired almost their initial speed and size.

to obtain acceleration has been switched off). We initialize the numerical simulations using the Ansatz

$$\mathbf{n}(x, y, 0) = \begin{cases} \mathbf{n}_v(x - a, y), & x \geq 0 \\ \mathbf{n}_v(x + a, y), & x < 0, \end{cases} \quad (13)$$

where  $\mathbf{n}_v$  is the traveling solution in Eq. (10) and  $a$  is a constant. Ansatz (13) represents two skyrmions at positions  $(\pm a, 0)$  at  $\tau = 0$ , each one has a speed  $v$  and they are on a collision course. We typically choose  $a = 10.5$  in the simulations. The auxiliary fields are given by Eq. (8). Specifically, the magnetization is

$$\mathbf{m}(x, y, 0) = \begin{cases} \frac{\epsilon v}{2\sqrt{2}} \mathbf{n} \times \partial_1 \mathbf{n}, & x \geq 0 \\ -\frac{\epsilon v}{2\sqrt{2}} \mathbf{n} \times \partial_1 \mathbf{n}, & x < 0. \end{cases} \quad (14)$$

The corresponding spin configuration is reconstructed by inverting Eqs. (4), and the simulation is performed on the spin lattice. For the time evolution, we use Eqs. (2). Our typical numerical mesh is  $1400 \times 700$ . Since,  $\epsilon = 0.03$ , the lattice extends in space in  $-21 < x < 21$ ,  $-10.5 < y < 10.5$ . Simulations performed on a larger lattice did not show any change in the results.

Figure 2 shows snapshots of the Néel vector configuration for a head-on collision of skyrmions with initial velocities  $v = 0.2$  [37]. Only the central part of the numerical mesh is shown in the snapshots. The skyrmions are initially at positions  $(\pm 10.5, 0)$ . The first snapshot shows the skyrmions when they are far enough from each other and they are not yet interacting. The second snapshot shows that, after approaching each other, the size of both skyrmions has been reduced, due to the interaction. Their velocity is reduced, too. The third snapshot shows the skyrmions at the minimum distance when their velocity is almost zero, while their size has further been reduced. After this moment, the skyrmions bounce back, their speed increases and their size is growing, too. The last snapshot shows the skyrmions when they are at a large distance from each other and they have been restored to almost their original profile, size, and speed.

Figure 3 presents the results of a second simulation for initial velocity  $v = 0.4$  [37]. The simulation results are similar to the case of  $v = 0.2$  in Fig. 2. But, the skyrmions, at the distance of minimum separation, shown in the third snapshot, have reached a minimum size that is now smaller. The phenomenon of bouncing back of skyrmions after a collision has been noted in [29] in a  $\sigma$  model with Skyrme-like terms.

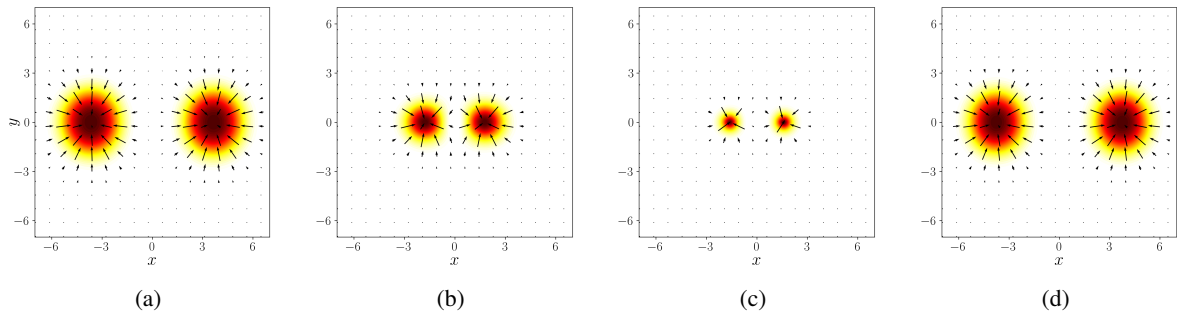


Figure 3: Simulation of a head-on collision of skyrmions placed initially ( $\tau = 0$ ) at positions  $(\pm 10.5, 0)$  with velocities  $v = \mp 0.4$ . The process is similar to Fig. 2. We show snapshots at times (a)  $\tau = 17.1$ , (b)  $\tau = 23.7$ , (c)  $\tau = \tau_{\text{crit}} = 27.1$ , where the skyrmions have approached closer and their size is smaller compared to the corresponding picture in Fig. 2, (d)  $\tau = 37.2$ .

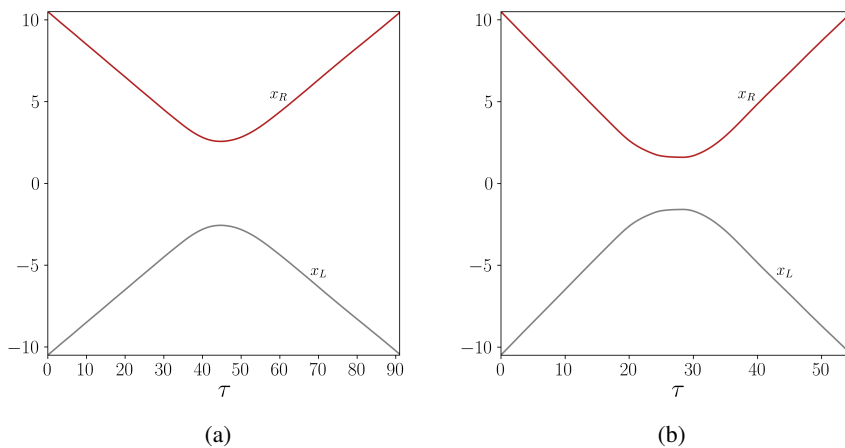


Figure 4: The position of the two colliding skyrmions on the  $x$  axis ( $x_L, x_R$  for the skyrmions coming from the left and right, respectively) as a function of time for initial velocities (a)  $v = 0.2$ , corresponding to the simulation in Fig. 2, and (b)  $v = 0.4$ , corresponding to the simulation in Fig. 3. The skyrmions stop temporarily and bounce back after the collision.

Figure 4 shows the positions of the skyrmions on the  $x$  axis with respect to time. For the skyrmion position, we find the two points on the  $x$ -axis where  $n_3 = 0$  and take the middle point between the two. The slope of the curves shows that the skyrmions acquire almost their initial velocity after bouncing back. For initial velocity  $v = 0.2$ , we have a velocity after bouncing back  $v = 0.192$ , and for initial velocity  $v = 0.4$ , we have  $v = 0.384$  after bouncing back. The minimum distance reached when they approach is smaller for the higher velocity case,  $v = 0.4$ , compared to the case  $v = 0.2$ .

Figure 5 shows the radius of the skyrmions during the collision. The radius is calculated as half the distance between the two points on the  $x$  axis where  $n_3 = 0$ , for each skyrmion. The skyrmion radius is almost constant before the collision, it reduces significantly during the collision and it is later restored to its initial size. After the collision, the skyrmion radius oscillates, clearly indicating that the breathing mode [38, 34] has been excited. The numerical simulations show that the decrease in the skyrmion size due to the interaction is a generic phenomenon. The small oscillations are mainly attributed to the error introduced by

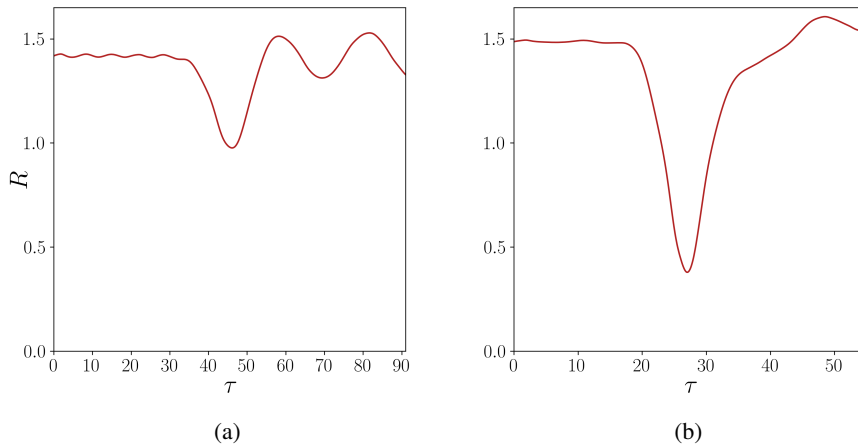


Figure 5: The radius of the skyrmions during the collision for the cases with initial velocities (a)  $v = 0.2$ , shown in Fig. 2, (b)  $v = 0.4$ , shown in Fig. 3.

the transformation of variables from the tetramers, where the solitary wave solutions have been found, to the spin lattice, where the simulations are performed.

A qualitative description of the skyrmion dynamics can be given by following the evolution of the energy terms. When the skyrmions approach, they decelerate, and their kinetic energy is converted to potential energy. This can be considered to consist of internal and interaction energy. The internal energy of the skyrmions is increasing as the skyrmion size is decreasing (for example, for  $\lambda = 0.50$ , the minimum potential energy is achieved for a static skyrmion with radius  $R = 1.40$ ). Fig. 6 shows the evolution of the energy terms for the simulation in Fig. 2 with initial skyrmion velocity  $v = 0.2$ . The DM and anisotropy energies are decreasing in absolute value as the size of the skyrmions decreases during the collision, while the exchange energy approaches its minimum possible value which is  $8\pi$ . The kinetic energy is shown in Fig. 6b and it approaches zero (to within numerical accuracy) at the time of minimum distance between the skyrmions.

The calculation of the energy terms is based on the formulas for the potential energy terms on the spin lattice (1). The kinetic energy, which is only meaningful in the continuum theory, has to be defined in a consistent way on the spin lattice. This is accomplished in Appendix A and the formula for the kinetic energy  $E_{\text{kin}}$  calculated via the spin vectors is given in Eq. (A.4). The exchange energy plotted in Fig. 6 is  $E_a = E_a^d - E_{\text{kin}}$ , while the DM and anisotropy terms are calculated using the formulas in Eq. (1), that is, we use the approximations  $E_{\text{ex}} = E_{\text{ex}}^d$ ,  $E_{\text{DM}} = E_{\text{DM}}^d$ .

We have performed simulations of head-on collisions also with higher initial skyrmion velocities. For example, we choose an initial velocity  $v = 0.56$  [37]. From Fig. 1, we see that such propagating skyrmions have energy  $E > 4\pi$  each, which is a crucial energy bound. Simulations show that such fast-moving skyrmions approach each other and their size decreases until they become very small with a size comparable to the lattice spacing. The skyrmions are then annihilated and the energy is eventually converted to spin waves. The collapse of solitons has been studied rigorously within certain models in [39, 40], while a skyrmion annihilation phenomenon within the present model was discussed in [34].

The process can be understood based on the conversion of kinetic energy to exchange energy. Since each skyrmion has a total energy  $E > 4\pi$ , the conversion of kinetic to potential energy is continuing during

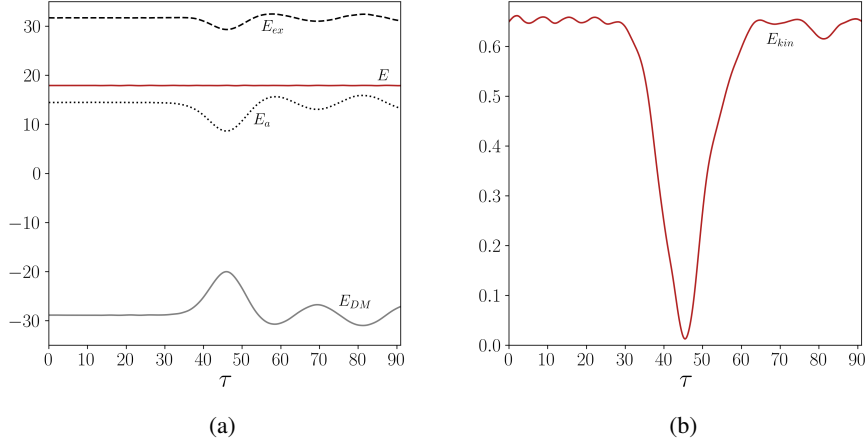


Figure 6: The evolution of the energy terms for the simulation of the collision of skyrmions with initial velocity  $v = 0.2$ . (a) The total energy  $E$  is conserved during the collision. Also plotted are the exchange, DM, anisotropy energy, and (b) the kinetic energy.

collision until the skyrmion has an infinitesimally small size with exchange energy  $E_{\text{ex}} = 4\pi$  and  $E_{\text{DM}} = 0$ ,  $E_{\text{a}} = 0$ . This is observed to happen in all simulations with large skyrmion initial velocities for which the energy of each of the initial propagating skyrmions is  $E > 4\pi$ . Different outcomes of the simulations, such as a combination of propagation and breathing of skyrmions cannot easily be excluded by theory arguments, however, no other outcome has been observed in our simulation other than the eventual skyrmion annihilation.

The generic phenomenon of skyrmion shrinking during collision is a challenging one and it should be explained in order to have a full theoretical picture of skyrmion collisions. On a descriptive level, we note that the interaction is due to the overlap of the far field of one skyrmion with the core of the other. One can claim that the far field of each skyrmion overlaps stronger with the side of the other one which is closer. Due to repulsive forces, the sides of the skyrmions that are closer to each other are decelerated stronger producing the skyrmion shrinking effect. Eventually, the complete skyrmion configuration decelerates as we have seen earlier. On a phenomenological level, the phenomenon seems similar to the squeezing of two elastic balls during their collision, except that the skyrmions interact already before their cores touch each other.

A partial analytical explanation of the process can be obtained if we start from the equation for the magnetization

$$\dot{\mathbf{m}} = \frac{\epsilon}{2\sqrt{2}} \mathbf{n} \times \mathbf{f} \quad (15)$$

that is an equivalent form of Eq. (6) obtained by using Eq. (8). In a heuristic approach, let us denote by  $\mathbf{f}_1, \mathbf{f}_2$  the effective fields due to the two skyrmion configurations. In the area around the core of, say, the left skyrmion, we have  $\mathbf{f}_2 \ll 1$ , and we may thus write the effective field in this area as  $\mathbf{f} \approx \mathbf{f}_1 + \mathbf{f}_2$  (that is, a small correction is added linearly to  $\mathbf{f}_1$  in order to get the full field  $\mathbf{f}$ ). We have

$$\dot{\mathbf{m}} = -\frac{\epsilon}{2\sqrt{2}} \mathbf{n} \times (\mathbf{f}_1 + \mathbf{f}_2)$$

which is describing the interaction of the far field of the right skyrmion impacted at the core region of the left skyrmion. At this point, remember that nonzero magnetization indicates dynamical behavior for the



Néel vector, as seen in Eq. (8). The main term  $\mathbf{n} \times \mathbf{f}_1$  gives the magnetization behavior necessary for the propagation of the left skyrmion with a constant velocity. The smaller term  $\mathbf{n} \times \mathbf{f}_2$  gives the interaction of the right skyrmion through its far-field with the left skyrmion. This is expected to decelerate skyrmion 1 due to the interaction being repulsive. Assuming that  $\mathbf{f}_2$  is larger on the side of skyrmion 1 which is closer to skyrmion 2, the effect on  $\dot{\mathbf{m}}$  is stronger on this side causing the squeezing of the skyrmion. The above heuristic approach shows that skyrmion shrinking during a collision can be expected to be a generic phenomenon.

#### 4. Conclusions

Exploiting the solitary wave properties of skyrmions in antiferromagnets, we have studied head-on collisions between two skyrmions. As a result of the interaction, skyrmions reduce their size and two outcomes are possible. Skyrmions that have an energy  $E < 4\pi$  collide and bounce back eventually almost restoring their initial speed. Skyrmions that have an energy  $E > 4\pi$  shrink as they approach until they concentrate to a point and disappear. We describe the collision process and explain the main feature by following the kinetic energy within the sigma model for antiferromagnets. For the calculation of the kinetic energy, we have derived a formula in terms of the spin vectors in the magnetic system.

While observations of skyrmions are abundant in ferromagnets, the observation of antiferromagnetic domains is still challenging. Given the rapid development of experimental techniques for the observation of antiferromagnetic order, we may reasonably expect that the creation and observation of skyrmions will be achievable in the next generation of experiments. The dynamical behavior of skyrmions in antiferromagnets is dramatically different than in ferromagnets. The results presented in this paper show how these dynamics couple with interactions between skyrmions to produce behaviors that have not been observed or predicted before in magnetic materials.

#### Acknowledgements

This work was supported by the project ‘‘ThunderSKY’’ funded by the Hellenic Foundation for Research and Innovation and the General Secretariat for Research and Innovation, under Grant No. 871.

#### Appendix A. Continuum energy from the energy of the spin lattice

We can obtain the continuous form of the energy (9) from the discrete form (1). The tetramerization of the lattice is shown in Fig. A.7.

For the exchange energy in the discrete, it is sufficient to consider the interactions between the spins in each tetramer. There are four terms and they can be compactly written as

$$(\mathbf{A} + \mathbf{C}) \cdot (\mathbf{B} + \mathbf{D}) = 4s^2(\mathbf{m} + \mathbf{n}) \cdot (\mathbf{m} - \mathbf{n}) = 4s^2(\mathbf{m}^2 - \mathbf{n}^2) = 4s^2(2\mathbf{m}^2 + \mathbf{k}^2 + \mathbf{l}^2 - 1).$$

In order to take into account also the interaction with spins in neighboring tetramers, we have to double the above result. For small  $\epsilon$ , we can obtain a continuum approximation by setting

$$\sum_{\alpha\beta} \rightarrow \frac{1}{(2\epsilon)^2} \int d^2x. \quad (\text{A.1})$$

The exchange energy in the discrete is then approximated as

$$E_{\text{ex}}^d \approx 8Js^2 \frac{1}{(2\epsilon)^2} \int (2\mathbf{m}^2 + \mathbf{k}^2 + \mathbf{l}^2) d^2x = Js^2 \frac{1}{2} \int (\dot{\mathbf{n}}^2 + \mathbf{n}_x^2 + \mathbf{n}_y^2) d^2x = Js^2 (E_{\text{kin}} + E_{\text{ex}}) \quad (\text{A.2})$$

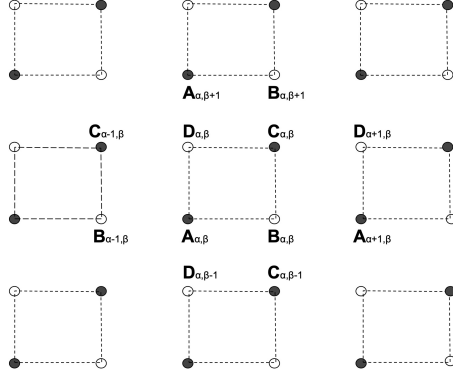


Figure A.7: A tetramerization of the square lattice. The tetramers are indexed by integers  $\alpha, \beta$  and the spins at each tetramer are denoted by  $A, B, C, D$ .

where we omitted a constant and used Eq. (8). Eq. (A.2) gives the decomposition of the exchange energy in the discrete to the kinetic and exchange energy in the continuum. A more elaborate approach where the interaction of spins of one tetramer are involved in the calculation explicitly, gives the same result (A.2), and we will thus not give it in detail here.

We may now derive a formula for the kinetic energy so that it can be calculated over the numerical mesh used in simulations. Using Eq. (8), we have

$$\mathbf{m} = \frac{\epsilon}{2\sqrt{2}} \mathbf{n} \times \dot{\mathbf{n}} \Rightarrow \mathbf{m}^2 = \frac{\epsilon^2}{8} \dot{\mathbf{n}}^2,$$

that is substituted in Eq. (9) for the kinetic energy of the continuum model, to give

$$E_{\text{kin}} = \frac{4}{\epsilon^2} \int \mathbf{m}^2 d^2x. \quad (\text{A.3})$$

The form for calculations on the numerical mesh is obtained by applying the substitution (A.1),

$$E_{\text{kin}} \approx 16 \sum_{\alpha,\beta} (\mathbf{m}_{\alpha,\beta})^2. \quad (\text{A.4})$$

A second, equivalent, formula can be derived for the kinetic energy. Eq. (8) for  $\mathbf{m}$  is equivalent to

$$\epsilon \dot{\mathbf{n}} = 2\sqrt{2} \mathbf{n} \times \mathbf{m} \Rightarrow \epsilon \dot{\mathbf{n}} = \frac{1}{2\sqrt{2}} [(\mathbf{A} + \mathbf{C}) \times (\mathbf{B} + \mathbf{D})] \quad (\text{A.5})$$

where we have used the definitions of  $\mathbf{m}, \mathbf{n}$  in Eq. (4). A form for the calculation of the kinetic energy (A.4) on the numerical mesh is obtained by applying (A.1),

$$E_{\text{kin}} = \frac{1}{2} \int \dot{\mathbf{n}}^2 d^2x \approx \frac{1}{4} \sum_{\alpha,\beta} [(\mathbf{A}_{\alpha,\beta} + \mathbf{C}_{\alpha,\beta}) \times (\mathbf{B}_{\alpha,\beta} + \mathbf{D}_{\alpha,\beta})]^2. \quad (\text{A.6})$$

For completeness, we will give the relation between the discrete and continuum energy for the DM and

anisotropy terms. For the DM energy, we write

$$\begin{aligned}
E_{\text{DM}}^d &= D \sum_{\alpha,\beta} [\hat{\boldsymbol{e}}_2 \cdot [\mathbf{B}_{\alpha,\beta} \times (\mathbf{A}_{\alpha+1,\beta} - \mathbf{A}_{\alpha,\beta}) + \mathbf{C}_{\alpha,\beta} \times (\mathbf{D}_{\alpha+1,\beta} - \mathbf{D}_{\alpha,\beta})] \\
&\quad - \hat{\boldsymbol{e}}_1 \cdot [\mathbf{D}_{\alpha,\beta} \times (\mathbf{A}_{\alpha,\beta+1} - \mathbf{A}_{\alpha,\beta}) + \mathbf{C}_{\alpha,\beta} \times (\mathbf{B}_{\alpha,\beta+1} - \mathbf{B}_{\alpha,\beta})] \\
&\approx 2Ds^2 \sum_{\alpha,\beta} \hat{\boldsymbol{e}}_1 \cdot (\mathbf{n}_{\alpha,\beta} \times \mathbf{n}_{\alpha+1,\beta}) - \hat{\boldsymbol{e}}_2 \cdot (\mathbf{n}_{\alpha,\beta} \times \mathbf{n}_{\alpha+1,\beta})
\end{aligned}$$

where we have retained only the lowest order terms in the last equation. Applying Eq. (A.1), we obtain

$$E_{\text{DM}}^d \approx Js^2 E_{\text{DM}}. \quad (\text{A.7})$$

For the anisotropy energy, we write

$$\begin{aligned}
E_a^d &= \frac{K}{2} \sum_{\alpha,\beta} (A_{\alpha,\beta,3}^2 + B_{\alpha,\beta,3}^2 + C_{\alpha,\beta,3}^2 + D_{\alpha,\beta,3}^2) \\
&= 2Ks^2 \sum_{\alpha,\beta} (n_{\alpha,\beta,3}^2 + m_{\alpha,\beta,3}^2 + k_{\alpha,\beta,3}^2 + l_{\alpha,\beta,3}^2) \approx 2Ks^2 \sum_{\alpha,\beta} n_{\alpha,\beta,3}^2
\end{aligned}$$

where subscript 3 denotes the third component of each vector, and we have retained only the lowest-order terms in the last equation. The continuum approximation is

$$E_a^d \approx \frac{Ks^2}{\epsilon^2} \left[ \frac{1}{2} \int (n_3)^2 d^2x \right] = Js^2 E_a. \quad (\text{A.8})$$

## References

- [1] A. V. Kimel, A. Kirilyuk, A. Tsvetkov, R. V. Pisarev, and T. Rasing, *Nature* **429**, 850 (2004).
- [2] N. Kanda, T. Higuchi, H. Shimizu, K. Konishi, K. Yoshioka, and M. Kuwata-Gonokami, *Nature Communications* **2** (2011), 10.1038/ncomms1366.
- [3] C. Tzschaschel, K. Otani, R. Iida, T. Shimura, H. Ueda, S. Günther, M. Fiebig, and T. Satoh, *Phys. Rev. B* **95**, 174407 (2017).
- [4] P. Němec, M. Fiebig, T. Kampfrath, and A. V. Kimel, *Nature Physics* **14**, 229 (2018).
- [5] F. Schreiber, H. Meer, C. Schmitt, R. Ramos, E. Saitoh, L. Baldrati, and M. Kläui, *Phys. Rev. Appl.* **16**, 064023 (2021).
- [6] C. Schmitt, L. Baldrati, L. Sanchez-Tejerina, F. Schreiber, A. Ross, M. Filianina, S. Ding, F. Fuhrmann, R. Ramos, F. Maccherozzi, D. Backes, M.-A. Mawass, F. Kronast, S. Valencia, E. Saitoh, G. Finocchio, and M. Kläui, *Phys. Rev. Appl.* **15**, 034047 (2021).
- [7] H. Meer, S. Wust, C. Schmitt, P. Herrgen, F. Fuhrmann, S. Hirtle, B. Bednarz, A. Rajan, R. Ramos, M. A. Niño, M. Foerster, F. Kronast, A. Kleibert, B. Rethfeld, E. Saitoh, B. Stadtmüller, M. Aeschlimann, and M. Kläui, *Advanced Functional Materials* **n/a**, 2213536 (2023), <https://onlinelibrary.wiley.com/doi/pdf/10.1002/adfm.202213536>.
- [8] P. Stremoukhov, D. C. S. A. Safin, S. Nikitov, and A. Kirilyuk, *New Journal of Physics* **24**, 023009 (2022).
- [9] P. Wadley, B. Howells, J. Železný, C. Andrews, V. Hills, R. P. Campion, V. Novák, K. Olejník, F. Maccherozzi, S. S. Dhesi, S. Y. Martin, T. Wagner, J. Wunderlich, F. Freimuth, Y. Mokrousov, J. Kuneš, J. S. Chauhan, M. J. Grzybowski, A. W. Rushforth, K. W. Edmonds, B. L. Gallagher, and T. Jungwirth, *Science* **351**, 587 (2016).
- [10] S. Y. Bodnar, L. Šmejkal, I. Turek, T. Jungwirth, O. Gomonay, J. Sinova, A. A. Sapozhnik, H.-J. Elmers, M. Kläui, and M. Jourdan, *Nature Communications* **9** (2018).
- [11] T. Moriyama, K. Oda, T. Ohkochi, M. Kimata, and T. Ono, *Scientific Reports* **8**, 14167 (2018).
- [12] H. Meer, F. Schreiber, C. Schmitt, R. Ramos, E. Saitoh, O. Gomonay, J. Sinova, L. Baldrati, and M. Kläui, *Nano Letters* **21**, 114 (2020).
- [13] T. Kampfrath, A. Sell, G. Klatt, A. Pashkin, S. Mährlein, T. Dekorsy, M. Wolf, M. Fiebig, A. Leitenstorfer, and R. Huber, *Nature Photonics* **5**, 31 (2010).

- [14] T. Higuchi, N. Kanda, H. Tamaru, and M. Kuwata-Gonokami, *Phys. Rev. Lett.* **106**, 047401 (2011).
- [15] E. Rongione, O. Gueckstock, M. Mattern, O. Gomonay, H. Meer, C. Schmitt, R. Ramos, E. Saitoh, J. Sinova, H. Jaffrès, M. Mičica, J. Mangeney, S. T. B. Goennenwein, S. Geprägs, T. Kampfrath, M. Kläui, M. Bargheer, T. S. Seifert, S. Dhillon, and R. Lebrun, “Emission of coherent thz magnons in an antiferromagnetic insulator triggered by ultrafast spin-phonon interactions,” (2022), arXiv:2205.11965 [cond-mat.mes-hall] .
- [16] V. Grigorev, M. Filianina, Y. Lytvynenko, S. Sobolev, A. R. Pokharel, A. P. Lanz, A. Sapozhnik, A. Kleibert, S. Bodnar, P. Grigorev, Y. Skourski, M. Kläui, H.-J. Elmers, M. Jourdan, and J. Demsar, *ACS Nano* **16**, 20589 (2022).
- [17] V. G. Bar'yakhtar, M. V. Chetkin, B. A. Ivanov, and S. N. Gadetskii, *Dynamics of Topological Magnetic Solitons – Experiment and Theory* (Springer, Berlin, 1994).
- [18] A. Bogdanov and S. A., *Physics of the Solid State* **40**, 1350 (1998).
- [19] S. Komineas and N. Papanicolaou, *Nonlinearity* **11**, 265 (1998).
- [20] A. N. Bogdanov, U. K. Röbler, M. Wolf, and K.-H. Müller, *Phys. Rev. B* **66**, 214410 (2002).
- [21] S. Gao, H. D. Rosales, F. A. G. Albarracín, V. Tsurkan, G. Kaur, T. Fennell, P. Steffens, M. Boehm, P. Čermák, A. Schneidewind, E. Ressouche, D. C. Cabra, C. Rüegg, and O. Zaharko, *Nature* **586**, 37 (2020).
- [22] H. Jani, J.-C. Lin, J. Chen, J. Harrison, F. Maccherozzi, J. Schad, S. Prakash, C.-B. Eom, A. Ariando, T. Venkatesan, and P. G. Radaelli, *Nature* **590**, 74 (2021).
- [23] E. G. Galkina and B. A. Ivanov, *Low Temp. Phys.* **44**, 618 (2018).
- [24] S. Komineas and N. Papanicolaou, *SciPost Phys.* **8**, 086 (2020).
- [25] C. Jin, C. Song, J. Wang, and Q. Liu, *Applied Physics Letters* **109**, 182404 (2016), <https://doi.org/10.1063/1.4967006> .
- [26] H. Velkov, O. Gomonay, M. Beens, G. Schwiete, A. Brataas, J. Sinova, and R. A. Duine, *New Journal of Physics* **18**, 075016 (2016).
- [27] A. Salimath, F. Zhuo, R. Tomasello, G. Finocchio, and A. Manchon, *Phys. Rev. B* **101**, 024429 (2020).
- [28] N. Manton and P. Sutcliffe, *Topological Solitons* (Cambridge University Press, Cambridge, 2007).
- [29] M. Peyrard, B. Piette, and W. J. Zakrzewski, *Nonlinearity* **5**, 563 (1992).
- [30] B. Piette, B. Schroers, and W. Zakrzewski, *Nuclear Physics B* **439**, 205 (1995).
- [31] R. Leese, *Nuclear Physics B* **344**, 33 (1990).
- [32] S. Komineas, C. Melcher, and S. Venakides, *Nonlinearity* **33**, 2295 (2020).
- [33] A. Bernand-Mantel, C. B. Muratov, and T. M. Simon, *Phys. Rev. B* **101**, 045416 (2020).
- [34] S. Komineas and P. E. Roy, *Phys. Rev. Res.* **4**, 033132 (2022).
- [35] L. Shen, J. Xia, G. Zhao, X. Zhang, M. Ezawa, O. A. Tretiakov, X. Liu, and Y. Zhou, *Phys. Rev. B* **98**, 134448 (2018).
- [36] H. Corte-León, M. V. Khanjani, G. Jakob, M. Kläui, F. Garcia-Sanchez, C. Barton, and O. Kazakova, (2023), 10.21203/rs.3.rs-2458354/v1.
- [37] Animations of the simulation results available here .
- [38] V. P. Kravchuk, O. Gomonay, D. D. Sheka, D. R. Rodrigues, K. Everschor-Sitte, J. Sinova, J. van den Brink, and Y. Gaididei, *Phys. Rev. B* **99**, 184429 (2019).
- [39] P. Bizon, Y. N. Ovchinnikov, and I. M. Sigal, *Nonlinearity* **17**, 1179 (2004).
- [40] I. Rodnianski and J. Sterbenz, *Annals of Mathematics* **172**, 187 (2010).